Model-based correlation between change of electrical resistance and change of dislocation density of fatigued-loaded ICE R7 wheel steel specimens

Peter Starke, Saarbrücken, Frank Walther, Dortmund, and Dietmar Eifler, Kaiserslautern, Germany

Article Information

Correspondence Address
Dr.-Ing. Peter Starke
Chair of Non-Destructive Testing and Quality Assurance
Saarland University
Am Markt Zeile 4
66125 Saarbrücken, Germany
E-mail: peter.starke@uni-saarland.de

Keywords
ICE wheel steel, fatigue, cyclic deformation behavior, change in electrical resistance, dislocation density

Weight-optimized component design as well as a reliable estimation of the lifetime of metallic materials and components require a comprehensive understanding of fatigue processes and a systematic investigation of the underlying fatigue behavior. This becomes even more important when designing highly loaded components such as wheels of high-speed passenger railway systems. Typically, mechanical stress-strain hysteresis measurements and increasingly different types of temperature and electrical resistance measurements are used to characterize the fatigue behavior and fatigue processes. Here, electrical resistance measurements provide significant information as they allow the detection of microstructural changes, e. g., through changes in dislocation density and structure. In addition, electrical resistance measurements can be considered in load increase and constant amplitude tests with inserted load-free sequences and in service load tests to characterize damage progress. In this paper, characteristic values of the change in electrical resistance were determined for ICE R7 wheel steel specimens and correlated with dislocation density, which was load- and cycle-dependent and determined through transmission electron microscopy.

Besides the appropriate dimensioning and selection of materials, understanding cyclic deformation behavior is fundamental for the reliable and economical operation of fatigue-loaded components. This understanding is very closely linked to the microstructure and characterized by the complexity of interrelated processes. Cyclic loading causes micro- and macro-plastic deformation of metallic materials and, with cyclic softening and/or hardening processes, leads to the formation of characteristic dislocation structures and deformation characteristics that may be the initial point of fatigue cracks. Fatigue-induced property changes can lead to the initiation and propagation of cracks and finally to failure. Changes in mechanical material behavior during cyclic loading are usually characterized by evaluating the plastic strain amplitude $\varepsilon_{a,p}$ [1-2], which can be expressed as a function of the number of cycles N in so-called cyclic deformation curves. In the fatigue experiments described below, change in temperature ΔT [3-5] and change in electrical resistance ΔR [6-9] were determined with high precision. Methods of measuring the change in electrical resistance are also suitable for continuous application for complex components in load-free sequences in the sense of monitoring actual conditions or structural health (SHM). In addition to geometry, electrical resistance depends on specific electrical resistance (resistivity) ρ^*, which changes with plastic deformation due to variations in defect density e. g., dislocation structure and density. DC-based electrical resistance measurement is excellent for the evaluation of progressive fatigue damage [10]. Potential drop measurements are commonly used to characterize fatigue crack growth behavior. In contrast to the procedure presented in this paper, the electrical

resistance measurements recorded depend only on a crack-related change in specimen geometry and not on damage-induced change in the microstructure of a material, whereby the interpretation of the measurement curves generally requires different considerations [11]. This paper is based on a previous paper [10] published in German and has been substantially enlarged through the inclusion of load increase tests with and without load-free sequences as well as investigations on the interaction between crack development and electrical resistance. Furthermore, the principle of the specific testing procedure for fatigue tests with load-free sequences is explained in more detail.

Methods and material

Experimental technique. Load increase tests (LIT) and constant amplitude tests (CAT) were performed under stress control with a stress ratio of R = -1 at ambient temperature (AT), with a test frequency of f = 5 Hz and a triangular load-time function until the ultimate number of cycles $N_{limit} = 2 \times 10^6$ or specimen failure.

Figure 1 shows a schematic representation of the various experimental procedures used. In addition to load increase tests (LITs) and constant amplitude tests (CATs), tests were carried out using load-free sequences (σ = 0 MPa) to evaluate load- and temperature-independent measured values characterizing the current damage state. A LIT enables the description of cyclic stress-strain behavior and the estimation of fatigue strength by means of a single test. For this purpose, starting from amplitudes chosen significantly below the fatigue limit, stress amplitude is increased stepwise after each step until specimen failure and the material's response is characterized by different physical quantities M.

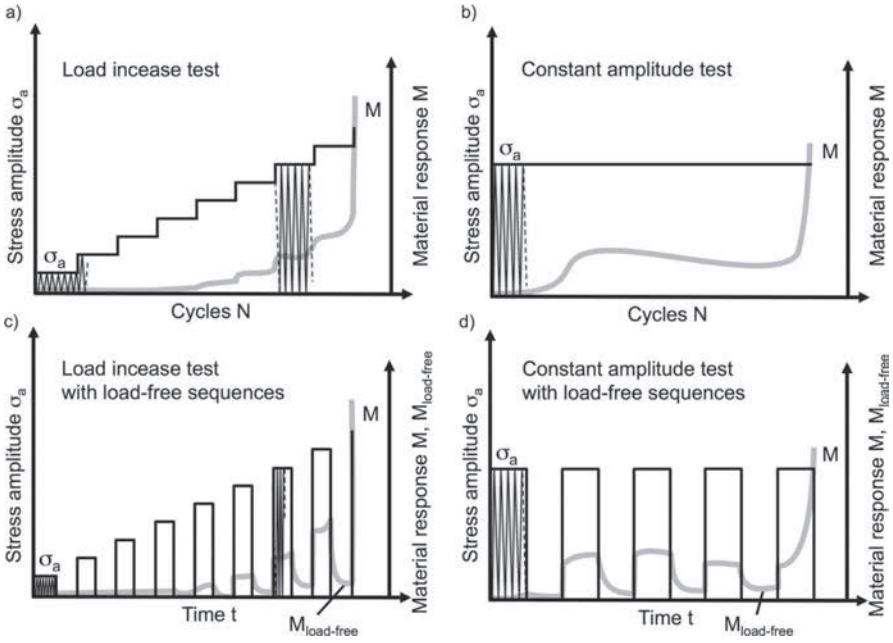

Figure 1: Schematic representation of the experimental procedures, a) load increase test, b) constant amplitude test, c) load increase test with load-free sequences, d) constant amplitude test with load-free sequences

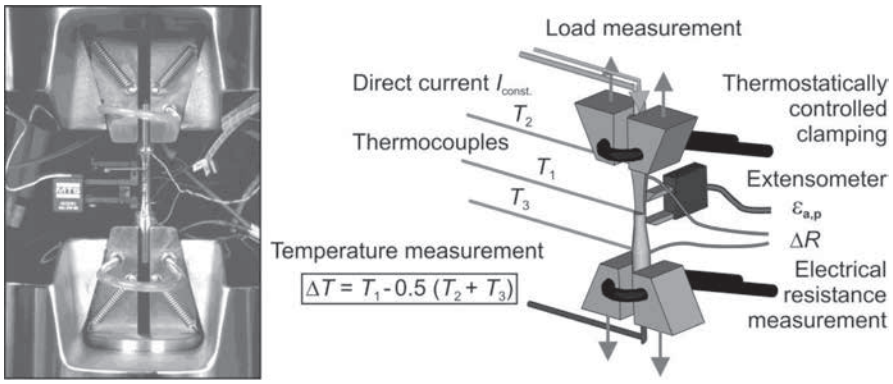

Figure 2: Photograph and schematic illustration of the experimental setup for mechanical stress-strain hysteresis, changes in temperature and electrical resistance measurements

The tests were carried out using a servo-hydraulic testing system type Schenck PSA 100 with an MTS Teststar IIs servo-controller at the Institute of Materials Science and Engineering at the University of Kaiserslautern. The load capacity of the testing system was 100 kN and the applied load cell enables measurements for force ranges +/- 10 kN, +/- 50 kN and +/- 100 kN with an accuracy of +/- 0.5 % of the measuring range set. For the investigations in this paper, a range of +/- 50 kN was used. Fatigue specimens with a cylindrical gauge length of 16 mm, a diameter of 7.6 mm and a notch factor of 1.00013 were used. The characterization of the fatigue behavior was based on mechanical stress-strain hysteresis, change in temperature and particularly change in electrical resistance measurements using a test setup shown in Figure 2 [12-13]. To prevent leakage of electric current through the machine frame with respect to the electrical resistance measurement, the grips were electrically isolated.

The change in temperature ΔT was measured using three thermocouples of type J, one in the middle of the gauge length (T_1) and two along the elastically loaded specimen shafts (T_2 and T_3). The theoretical background can be deduced from the consideration of the stress-strain hysteresis loop. The area of the hysteresis loop describes the cyclic plastic deformation energy which is transformed into internal energy U and heat energy Q. The internal energy enables microstructural changes in dislocation structure and density, voids and pores, and micro-cracks. The predominant proportion of 90 % to 95 % of the plastic deformation work dissipates as heat leads to an increase in specimen temperature [14].

For high sensitive resistometric measurements, the specimen was subjected to a direct current of I = 8 A and the change in electrical resistance ΔR was accurately measured using two wires spot-welded at the transition areas between the specimens' gauge length and the clamping shafts. For the connection to the data ac-

quisition device, copper cables with a cross section of 1.77 mm² and a length of 1,000 mm were used and the welding process was performed without additives in order to increase the reproducibility of electrical resistance measurements. The temperature influence on the electrical resistance was determined by a heating test providing the following relationship:

$$\Delta R/\Delta T = 0.402\ \mu\Omega \times K^{-1} \quad (1)$$

Besides small geometrical changes under mean stress-free loading, electrical resistance R depends in the range before microcrack initiation and macro-crack propagation exclusively on the specific electrical resistance ρ*, which is a function of deformation-induced microstructural changes. In addition to conventional load increase and constant amplitude tests, both test procedures were also carried out using discrete inserted load-free sequences (σ = 0 MPa) to determine the change in electrical resistance $\Delta R_{load\text{-}free}$ at ΔT = 0 K [10].

Material. The R7 wheels used in high-speed passenger trains and freight transport are manufactured in accordance with UIC standard-conforming heat treatment processes. The specimens were machined tangentially from wheel segments in rolling direction. The chemical composition of the unalloyed, lower eutectic steel corresponds to SAE 1050 to 1055 and is shown in Table 1 [10,12,15].

During the industrial heat treatment, the wheels' tread is cooled by spraying nozzles (see Figure 3a) using a water-based liquid in a so-called "rim chilling" heat treatment process. Based on the geometry and the mass of the wheel, varied cooling rates occur, resulting in locally dependent microstructures within the wheel [10,12,15]. The monobloc wheel has a width at the respective end faces from flange to tread of approx. 135 mm and a diameter from tread to tread of approx. 920 mm in the non-reprofiled original condition. Figure 3a shows a detail of the R7 wheel geometry, which is cut free at the transition to the wheel blade containing the investigated fatigue-relevant areas.

Figure 3b shows a ferritic-pearlitic microstructure in the tread area under a scanning electron micrograph (SEM) [16]. 14 specimens are machined tangentially from each wheel segment, which can be assigned to three characteristic functional component areas with comparable microstructural and mechanical properties (see Figure 3a). Figure 3c shows these characteristic values of the section in the tread area (A1), wear limit area (A2) and flange area (A3). The wear limit ranges between 25–35 mm as distance to the tread surface. It is marked using a dash in the diagram showing the wheel geometry (see Figure 3a). Next to the tread (A1), a ferrite content of 8 ar.-% (ar.: area), a cementite lamella spacing of 0.14 µm and a hardness of 275 HV10 were measured. The ferrite fraction and the cementite lamella spacing increase with increasing distance to the tread surface based on a decreasing cooling rate up to a maximum value of 15 ar.-% and 0.19 µm, respectively, in the flange (A3). The hardness drops down to 245 HV10 in A3 [10,12,15].

Mechanical properties derived from tensile and notch impact tests for the three cross-section areas A1 (tread) to A3 (flange) are presented in Table 2.

Results

Load increase and constant amplitude tests. Load increase tests (LIT) allow to es-

	Fe	C	Si	Mn	Cr	Cu	Mo	Ni
R7	97.91	0.53	0.32	0.75	0.26	0.04	0.01	0.11

Table 1: Chemical composition of wheel steel R7 in wt.-%

Parameters	A1	A2	A3
Yield strength R_e (MPa)	544	505	463
Tensile strength R_m (MPa)	902	850	826
Notch impact strength KCV (J × cm^{-2})	26	27	29

Table 2: Properties from tensile and notch impact tests of wheel steel R7

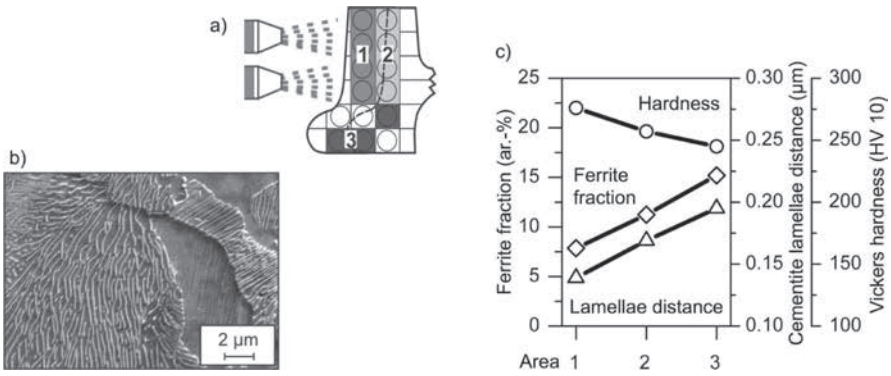

Figure 3: a) Schematic mapping of 14 specimen positions with respect to the cross-section areas (A)1 to 3, b) SEM micrograph of the tread (A1), c) position-specific (local) microstructural and hardness values for A1 to A3

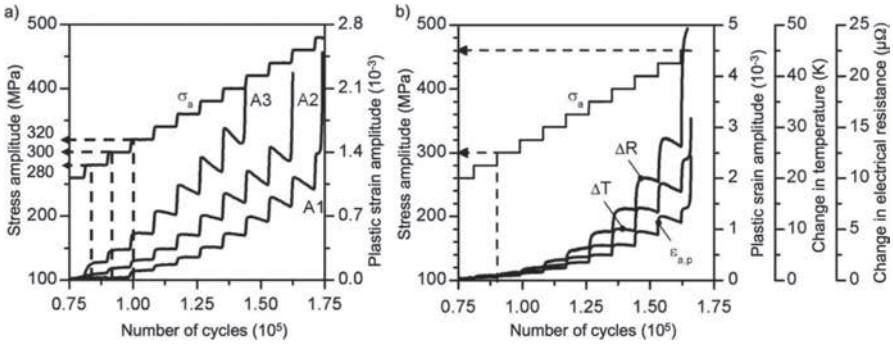

Figure 4: a) Development of plastic strain amplitude in a load increase test for A1, A2 and A3, b) development of plastic strain amplitude, change in temperature and change in electrical resistance in a load increase test for A2

timate the fatigue limit of a material through one single fatigue test. In Figure 4a, the stress amplitude σ_a, starting at $\sigma_{a,start}$ = 100 MPa with a stepwise increase of $\Delta\sigma_a$ = 20 MPa each $\Delta N = 9 \times 10^3$ cycles and the plastic strain amplitude $\varepsilon_{a,p}$ are plotted versus the number of cycles for specimens from area A1 (tread) to A3 (flange). The initial step can be set to $\sigma_{a,start} = 0.2 \times R_e$ which is valid for most low and medium carbon steel. For the specimens of the three cross-section areas, $\sigma_{a,start}$ was chosen at 100 MPa to allow for a comparison of the results. It can be verified that from this single test, the fatigue limit can be estimated in quite good accordance with the conventionally determined fatigue limit, which is expressed in Figure 6a. The assessment of the fatigue limit in the LIT provides a slightly conservative estimation with a congruence of about 90 % [12-13].

In addition, Figure 4b shows the plastic strain amplitude $\varepsilon_{a,p}$, the changes in temperature ΔT and electrical resistance ΔR as a function of the number of cycles for a specimen from wear limit area A2 in a LIT. The $\varepsilon_{a,p}$, ΔT and ΔR data represent equivalently the actual fatigue state and result in similar curves. The fatigue limit of A2 can be estimated by the determination of the transition point from predominantly elastic to elastic-plastic behavior which is characterized by a disproportional increase in $\varepsilon_{a,p}$, ΔT and ΔR values at $\sigma_{a,LIT}$ = 300 MPa, followed by the appearance of cyclic softening or cyclic softening/hardening due to increased stress amplitudes. Failure occurs in the LIT for A2 at σ_a = 460 MPa.

Figure 5a shows the cyclic deformation curves of constant amplitude tests (CAT) with a stress amplitude of σ_a = 400 MPa in terms of the plastic strain amplitude $\varepsilon_{a,p}$ vs. the number of cycles N, which represent the huge influence of the heat treatment-based local microstructure on cyclic deformation behavior and fatigue strength. As seen in the characteristic microstructural and quasi-static values (see Figure 3c), cyclic deformation curves can be classified as three characteristic areas: tread (A1), wear limit (A2) and flange (A3) based on the characteristic set of cyclic deformation curves (see Figure 5a).

The local cyclic deformation behavior is characterized by different incubation intervals with $\varepsilon_{a,p}$values close to zero until the first cyclic softening [10,12,17]. After passing the cyclic softening maximum, cyclic hardening leads to decreased plastic strain amplitudes until just before final failure. Macroscopic crack formation and propagation lead to a fictive secondary cyclic softening. With increasing distance between tread and flange, the increasing ferrite fraction and cementite lamella spacing result in earlier and more pronounced cyclic softening associated with reduced lifetime. The number of cycles to failure at identical stress amplitude differs by a decade: 1.6×10^4 cycles in flange (A3) and 1.7×10^5 cycles in tread (A1). To explain the influence of the microstructure on cyclic deformation behavior, Figure 5b shows the plastic strain amplitude at half lifetime $\varepsilon_{a,p}$ ($0.5 \times N_f$) and the number of cycles to failure N_f as a function of the ferrite fraction and the cementite lamella distance of the perlite. Ferrite fraction and cementite lamella distance, which increase both from tread to flange, result in an increase of the plastic strain amplitude and consequently in a reduction of lifetime.

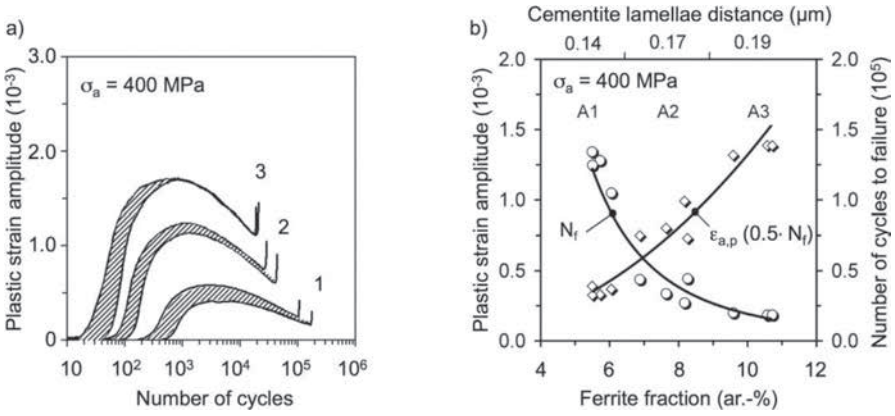

Figure 5: a) Cyclic deformation curves, b) influence of the ferrite fraction and cementite lamellae distance on the plastic strain amplitude and fatigue life for A1 to A3 specimens

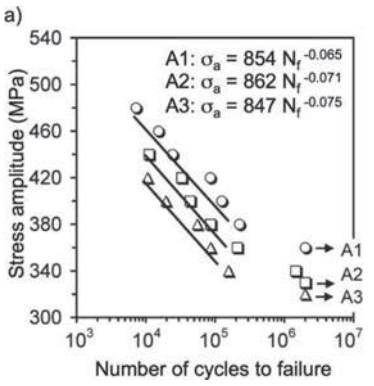

b)

	A1	A2	A3
$\sigma_{a,LIT}$ (MPa)	320	300	280
$\sigma_{a,CAT}$ (MPa)	360	330	320
$\sigma_{a,LIT}/\sigma_{a,CAT}$ (%)	89	91	88

Figure 6: a) S-N curves, b) fatigue limit evaluated in load increase (LIT) and constant amplitude tests (CAT) for specimens taken from areas A1 to A3

The pronounced influence of the microstructure on fatigue behavior can be further seen in the differences in the S-N curves as well as in the evaluated fatigue limits of areas A1-A3 (see Figure 6). The S-N curves are close to parallel and the fatigue strength for $N_{limit} = 2 \times 10^6$ ranges from 320 MPa (A3) to 360 MPa (A1). The resulting difference is approximately 11 %.

Since the description of the microstructure-property relationship was of prime importance, the S-N curves were determined through a step-down test procedure and not proven statistically.

Load increase and constant amplitude tests with load-free sequences. In addition to fatigue tests with continuous cycling until specimen failure, load increase and constant amplitude tests with well-defined load-free sequences (σ = 0 MPa) were performed, in order to determine the change in electrical resistance $\Delta R_{load\text{-}free}$ at ΔT = 0 K [10]. The change in electrical resistance detected in an unloaded condition therefore provides reproducible results for fatigue damage due to increasing defect density based on increasing $\Delta R_{load\text{-}free}$ values and is virtually unaffected by phonons (Matthiessen's rule).

Figure 7 shows the development of the plastic strain amplitude, the change in temperature and the change in electrical resistance as functions of time for a specimen of A2 in a stepwise LIT with load-free sequences (σ = 0 MPa).

The measurement methods applied are

equally suitable for fatigue assessment. After each load-free sequence, the values measured for the previous loading sequence are reached again when cyclizing is continued. This is a proof that the physical values measured depend exclusively on current loading and are not affected by the load-free sequences which can also be seen by comparing them to the results in Figure 4.

Figure 8 shows the same procedure with load-free sequences for a CAT at σ_a = 400 MPa. As shown in Figure 7 for the LIT, within a few cycles after the load-free sequence the measured values reach the same level than before, which underscores the fact that this test strategy results in comparable results for CATs with and without load-free sequences.

If, instead of a time-based plot (see Figure 8a), a plot for values measured vs. the number of cycles N is used (see Figure 8b), the data recorded during cyclic loading lead to the known representation of the $\varepsilon_{a,p}$-N, ΔT-N and ΔR-N cyclic deformation curves. Information on values measured recorded during load-free sequences is hereby lost in the process.

A maximum plastic strain amplitude of 1.0×10^{-3}, a change in temperature of 16.4 K, and a change in electrical resistance of 11.1 μΩ are noted at the stage of maximum cyclic softening after 5 % N_f ($N = 2.5 \times 10^3$) and $t = 1.2 \times 10^4$ s, respectively (see Figure 8). Due to cyclic hardening, decreasing $\varepsilon_{a,p}$, ΔT, and ΔR values are measured in the following loading sequences, where the decrease in ΔR values mostly depends on the decrease of the ΔT values.

The load-free sequences between the loading sequences are set in such a way that the deformation-induced change in temperature decreases to ΔT = 0 K, so that $\Delta R_{load\text{-}free}$ can be determined at the end of the load-free sequences without any temperature influences.

In Figure 9 the measured values of the load-free change in electrical resistance $\Delta R_{load\text{-}free}$ as functions of time t (a) and number of cycles N (b) for CATs with stress amplitudes between 400 and 460 MPa are plotted. $\Delta R_{load\text{-}free}$ increases exponentially, especially in the range of cyclic hardening (see Figure 9a). The increase is more pronounced with increasing stress amplitude. For σ_a = 460 MPa, a maximum change in electrical resistance of $\Delta R_{load\text{-}free}$ = 0.8 μΩ is reached in the load-free sequence just before specimen failure. Based on the electrical resistance of the non-damaged original state $R_{load\text{-}free,N=0}$, which is approximately 181 μΩ, this corresponds to an increase of $\Delta R_{load\text{-}free}/R_{load\text{-}free}$ = 0.44 %.

Figure 10 illustrates the change in electrical resistance ΔR (during cyclic loading) and the change in load-free electrical resistance $\Delta R_{load\text{-}free}$ (without cyclic loading at the end of the load-free sequence, ΔT = 0 K) (a) as well as the change in the specific electrical resistance $\Delta\rho^*$ (b) calculated from the load-free change in electrical resistance without temperature influence for stress amplitudes between 340 MPa and 440 MPa at a number of cycles $N = 10^4$. The cyclic stress-measurand-curves were evaluated equivalent to conventional cyclic stress-strain-curves and can be described based on a generalized Morrow equation [10,12-13,15,18]. Since the stress amplitudes increase, the changes in electrical resistance value likewise increase, which is expressed in the relationships shown in Figure 10a, where ΔR values are expected to be larger than the $\Delta R_{load\text{-}free}$ values. Figure 10c displays the relationship between the change in specific electrical resistance $\Delta\rho^*$ and load-free electrical resistance $\Delta R_{load\text{-}free}$ for a stress amplitude of σ_a = 400 MPa. The quotient $\Delta\rho^*/\Delta R_{load\text{-}free} = A/L$, where A is the cross-sectional area and L the length of the specimen's

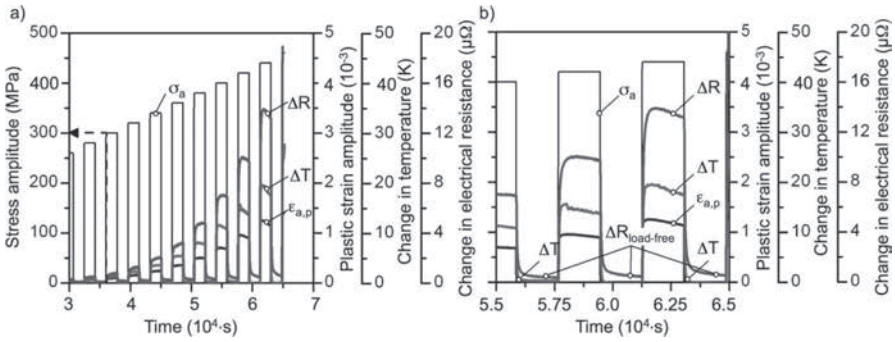

Figure 7: a) Stress amplitude, plastic strain amplitude, change in temperature and change in electrical resistance in a load increase test interrupted by load-free sequences as a function of time, b) detail

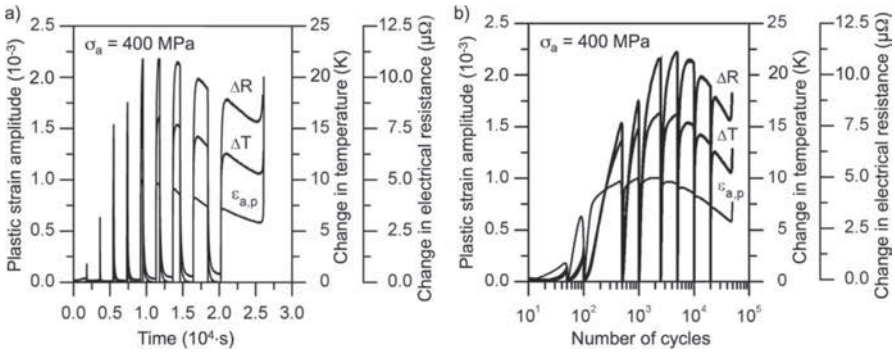

Figure 8: Plastic strain amplitude, change in temperature and change in electrical resistance in a constant amplitude test interrupted by load-free sequences a) as a function of time, b) as a function of number of cycles

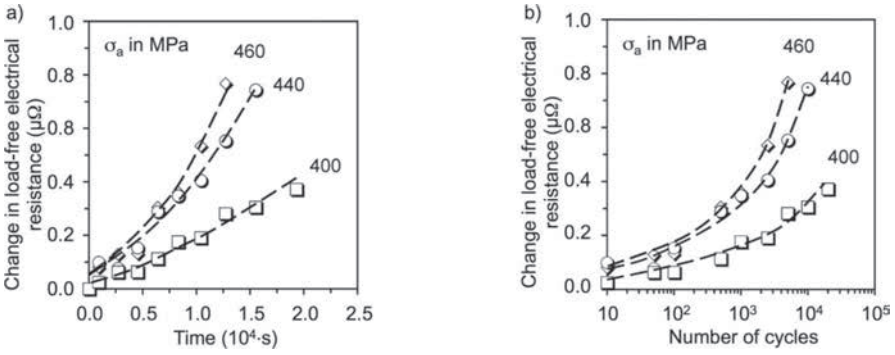

Figure 9: Change in load-free electrical resistance in constant amplitude tests interrupted by load-free sequences, a) as a function of time, b) as a function of number of cycles

gauge length, ranges from 2.88 to 2.90 mm. The specific electrical resistance ρ^* of the R7 steel is approximately 269 $\mu\Omega \times$ mm in the unloaded origin specimen state.

In the relationships in Figure 10, it is assumed that the volume and the quotient L/A remain constant, which means that advanced fatigue progress is mostly linked to crack propagation and the associated reduction of the effective specimen's cross-section, whereby close to specimen failure the $\Delta R_{load\text{-}free}$ values are over-estimated.

Load- and cycle-dependent quantitative investigation of the microstructure. Scanning electron micrographs (SEM) for specimens from flange (A3) and tread (A1) areas of R7 wheels are displayed vertically to the loading direction. During cyclic softening, the first slip lines and slip bands occur (see Figure 11a). After reaching the maximum of cyclic softening at 5 % N_f, in- and extrusions as well as first micro-cracks are observed. The micro-crack in Figure 11b is oriented under 45° to the loading direction, since the slip direction of favorably oriented slip systems often coincides with the direction of the macroscopically largest shear stress. Up to 85 % N_f, micro-cracks increase in the direction of the slip characteristics and the crack opening is more pronounced. In Figure 11c, it can be seen that the crack tips branched in the direction of the slip characteristics. After fracture, the surface was slightly etched in order to assign the crack profile to the materials' microstructure. The SEM image (see Figure 11d) is characterized by a high density of slip characteristics and the formation of crack systems along the grain boundaries is clearly visible (marked with black arrows).

Transmission electron microscopic (TEM) investigations (see Figure 12) are fundamental for an understanding and interpretation of the applied physically-based measurement methods and provide information regarding the change in dislocation structure as a function of the applied load and the number of cycles [10,16].

The dislocation structure and reactions have a significant influence on the specific electrical resistance ρ^*, which is directly linked to the electrical resistance via the quotient L/A. Since this ratio can be assumed to be almost constant for mean stress-free fatigue tests, there exists a direct relationship between dislocation structure, dislocation density and electrical resistance as well as between their changes.

The TEM investigations carried out at the Institute of Material Science at the Freiberg University of Mining and Technology show that in the initial state (N = 0 cycles), a homogeneous dislocation arrangement is present in the ferrite (see Figure 12a). The constant amplitude loading with σ_a = 400 MPa leads to significant changes in the dislocation arrangement and density (see Figure 12b). At the point of maximum cyclic softening (N ≈ 5 % N_f), long-stretched, partially venous cells are observed. This behavior of ferrite is very similar to that of normalized SAE 1045. The dislocation density within the dislocation cells is relatively low (see Figure 12b). Fatigue loading of up to 85 % N_f leads to a significant reduction in the diameters of the dislocation cells (see Figure 12c, d) [10, 16].

Figure 13 shows the relationship between the change in load-free electrical resistance $\Delta R_{load\text{-}free}$ and the dislocation density ρ_d (a) as well as the change in the dislocation density $\Delta\rho_d$ in relation to the initial state at N = 0 cycles (b). In addition to the initial state, the dislocation density in the stages of maximum cyclic softening and hardening was determined by radiographic profile analysis which integrated over a volume of about 0.5-1.0 mm³. The (211) reflex of bcc steel was measured by Co-Ka radiation. According to Fourier analysis, the values shown emerged from the Warren-Averbach and Krivoglaz-Wilkens plot [10,16].

Beside the initial state (N = 0 cycles, white symbols), pairs of values are specified for the state of maximum cyclic softening (N = 5 % N_f, grey symbols) and maximum cyclic hardening (N = 85 % N_f, black

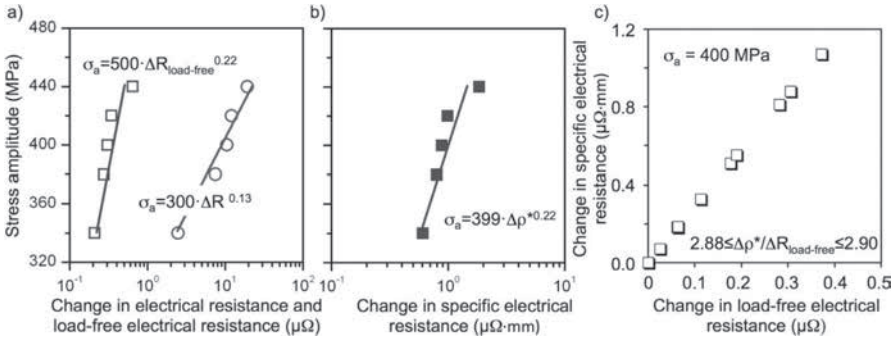

Figure 10: a) Relation between stress amplitude and change in electrical resistance as well as change in load-free electrical resistance, both measured at N = 10^4 cycles, b) relation between stress amplitude and calculated change in specific electrical resistance for N = 10^4 cycles, c) relation between calculated change in specific electrical resistance and change in load-free electrical resistance

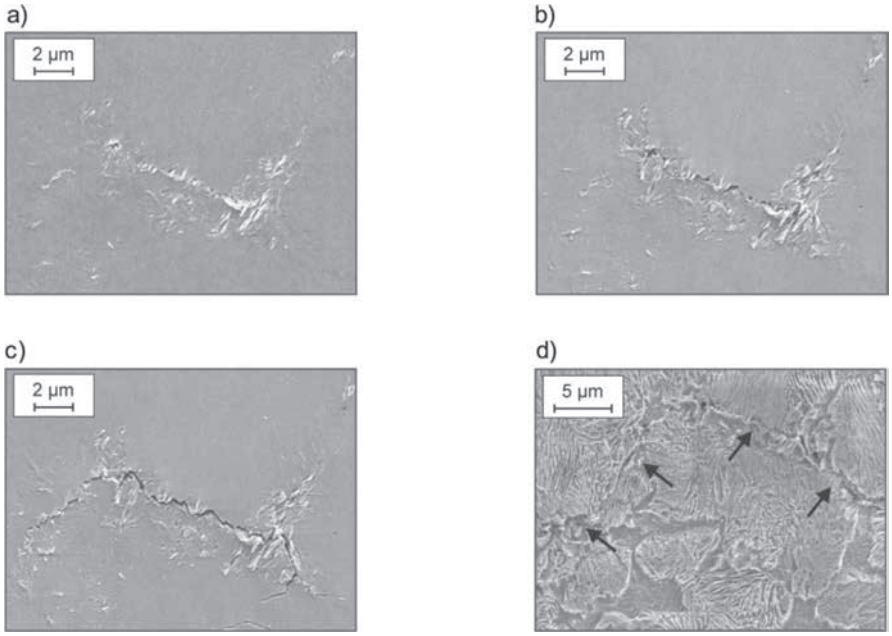

Figure 11: SEM images of a A3 specimen from the flange for a constant amplitude test at σ_a = 400 MPa after a) N = 5 % N_f, b) 50 % N_f, c) 85 % N_f and d) N_f (loading direction: ↕)

symbols) connected through trend lines for the investigated cross-section areas. Up to a fatigue state of 5 % N_f, which is characterized by a strong increase in the dislocation density compared to the initial state, the $\Delta R_{load\text{-}free}$ values increase up to 0.1 µΩ. The relationships between $\Delta R_{load\text{-}free}$ and ρ_d or $\Delta\rho_d$ between 5 % and 85 % N_f are characterized by a much steeper increase in the change in load-free electrical resistance up to 0.85 µΩ, with only small changes in the dislocation density. Consequently, different microstructural mechanisms dominate the increasing change in the load-free electrical resistance depending on the fatigue state. It can be assumed that up to 5 % N_f, the increasing dislocation density is responsible for the comparatively slight increase in the change in electrical resistance and furthermore up to 85 % N_f, microcrack formation and propagation are decisive for the sharp increase in the change in electrical resistance [10,16].

In Figure 14 the relationship between the microstructure, the dislocation density, and the change in the load-free electrical resistance is shown in detail at the stage of maximum cyclic softening (N = 5 % N_f) with the aim of visualizing the microstructure-property relation.

For R7 wheels, the accelerated cooling of the tread (A1) during industrial heat treatment leads to a smaller ferrite content and cementite lamella distance as well as approx. the doubling of the dislocation density (see Figure 14a) compared to the flange (A3). After fatigue loading with σ_a = 400 MPa up to 5 % N_f, the dislocation densities still differ by 25 % (see Figure 14b). The larger ferrite content and lamella distance in the flange result in significantly greater plastic deformation, which is reflected in higher values of the plastic strain amplitude $\varepsilon_{a,p}$, change in temperature ΔT and change in load-free electrical resistance $\Delta R_{load\text{-}free}$ (see Figure 14b) as well as a shorter lifetime N_f (see Figure 5a) compared to the tread. The relationship between the mechanical, thermal and electrical measurement values, which further underlines the suitability and interaction of the physical methods applied for the characterization of fatigue behavior and damage state, is obvious.

Conclusions

In short, it can be stated that electrical resistance or its change is well suited to characterize fatigue-induced deformation and damage processes. Here, the electrical resistance method offers the advantage that even small microstructural changes, which are reflected in the changes of the dislocation structure and density, can be detected. In addition, these methods can be applied in load-free sequences in the sense of structural integrity inspection methods. Temperature-unaffected load-free electrical resistance measurements are very well suited for an accurate and reproducible analysis of deformation-induced microstructural changes and damage progressions.

The investigations on ICE R7 wheel specimens show that between the states of

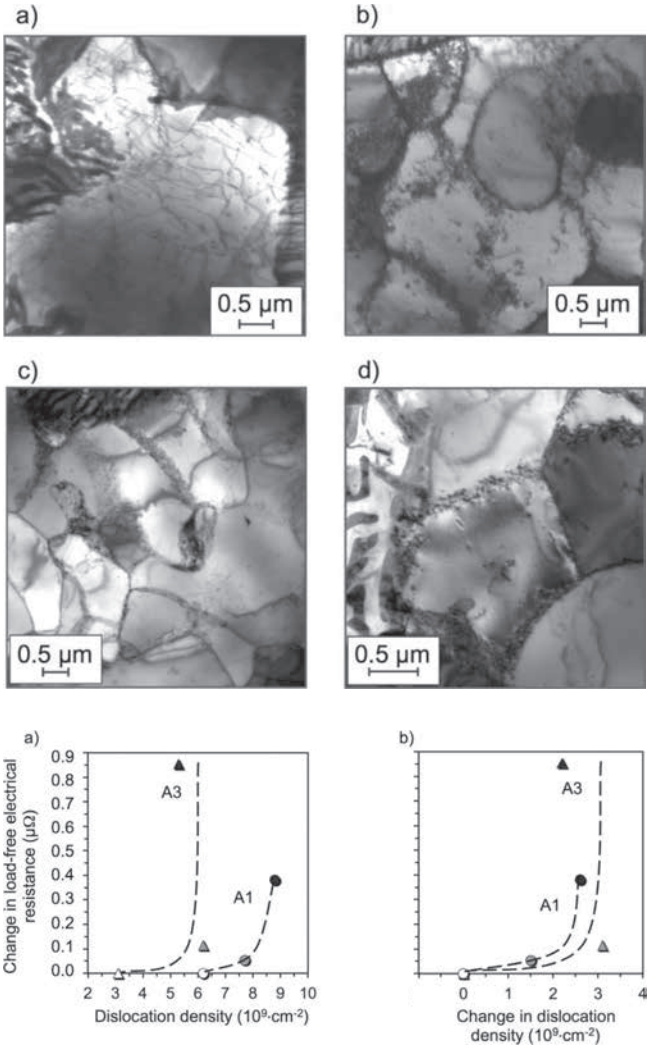

Figure 12: TEM micrographs of specimens a) of the tread (A1) in the original state N = 0, b) of the flange (A3) for a constant amplitude test with σ_a = 400 MPa after N = 5 % N_f, c) of the wear limit (A2), d) of the flange (A3), both for σ_a = 400 MPa after N = 85 % N_f

Figure 13: Specimens of tread (A1) and flange (A3) areas, data points filled white for N = 0 cycles, filled grey for N = 5 % N_f and filled black for N = 85 % N_f, a) relation between the change in load-free electrical resistance and dislocation density for σ_a = 400 MPa, b) relation between the load-free electrical resistance and change in dislocation density for σ_a = 400 MPa

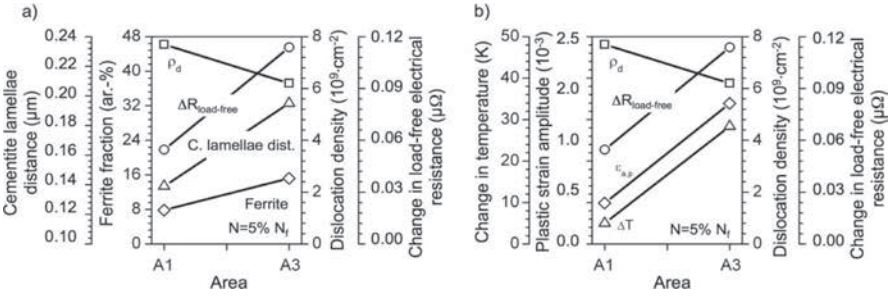

Figure 14: Specimens of tread (A1) and flange (A3) areas for σ_a = 400 MPa at N = 5 % N_f, a) microstructural parameters, change in load-free electrical resistance and dislocation density, b) plastic strain amplitude, change in temperature, change in load-free electrical resistance and dislocation density

maximum cyclic softening and maximum cyclic hardening, only relatively small changes in dislocation density take place, whereas the load-free change in electrical resistance increases by up to 16 times. As illustrated by transmission electron microscopic investigations, there are changes in the dislocation structure, e. g., decreasing cell diameters in this range of number of cycles, which limit the distances and the possibilities of dislocation movement. In addition, formation and propagation of micro-cracks are intensified. Load-free electrical resistance and its changes integrate over-all microstructural changes occurring in the material and are able to integrally depict the defect density of the material based on progressive fatigue damage.

Acknowledgement

The authors kindly thank the German Research Foundation (Deutsche Forschungsgemeinschaft, DFG) for financial support for this research work.

Extracts of this paper were published in German in [10] on the occasion of the 65th birthday of Prof. Dr. Dietmar Eifler.

References

1 P. Lukáš, M. Klesnil: Cyclic stress-strain response and fatigue life of metals in low amplitude region, Materials Science and Engineering 11 (1973), pp. 345-356, DOI: 10.1016/0025-5416(73)90125-0

2 A. Brazenas, D. Vaiciulis: Determination of fatigue curve parameters at cyclic strain limited loading according to the mechanical characteristics of power energy structural materials, Nuclear Engineering and Design 241 (2011), pp. 3596-3604, DOI: 10.1016/j.nucengdes.2011.07.022

3 F. Curà, A. E. Gallinatti, R. Sesana: Dissipative aspects in thermographic methods, Fatigue and Fracture of Engineering Materials & Structures 35 12 (2012), pp. 1133-1147, DOI: 10.1111/j.1460-2695.2012.01701.x

4 G. Meneghetti, R. B. Atzori: A two-parameter, heat energy-based approach to analyze the mean stress influence on axial fatigue behavior of plain steel specimens, International Journal of Fatigue 60–70 (2016), pp. 60-70, DOI: 10.1016/j.ijfatigue.2015.07.028

5 D. Rigon, M. Ricotta, G. Meneghetti: An analysis of the specific heat loss at the tip of severely notched stainless steel specimens to correlate the fatigue strength, Theoretical and Applied Fracture Mechanics 92 (2017), pp. 240-251, DOI: 10.1016/j.tafmec.2017.09.003

6 M. A. Omari, I. Sevostianov: Evaluation of the growth of dislocations density in fatigue loading process via electrical resistivity measurements, International Journal of Fracture 179 (2013), pp. 229-235, DOI: 10.1007/ s10704-012-9780-5

7 O. Glushko, M. J. Cordill: Electrical Resistance Decrease Due to Grain Coarsening Under Cyclic Deformation, JOM 66, 4 (2014), pp. 598-601, DOI: 10.1007/s11837-014-0943-x

8 M. A. Omari, I. Sevostianov: Estimation of changes in the mechanical properties of stainless steel subjected to fatigue loading via electrical resistance monitoring,International Journal of Engineering Science 65 (2013), pp. 40-48, DOI: 10.1016/j.ijengsci.2013.02.006

9 B. Sun, L. Yang, Y. Guo: A high-cycle fatigue accumulation model based on electrical resistance for structural steels, Fatigue and Fracture of Engineering Materials & Structures 30 (2007), pp. 1052-1062, DOI: 10.1111/j.1460-2695.2007.01175.x

10 P. Starke, F. Walther: Modellbasierte Korrelation zwischen dem elektrischen Widerstand und der Versetzungsstruktur des ermüdungsbeanspruchten ICE-Radstahls R7, Materials Testing 57 (2015), No. 1, pp. 9-16, DOI: 10.3139/120.110681

11 C. Motz, O. Friedl, R. Pippan: Fatigue crack propagation in cellular metals, International Journal of Fatigue 27, 10-12 (2005), pp. 1571-1581, DOI: 10.1016/j.ijfatigue.2005.06.044

12 F. Walther, D. Eifler: Fatigue life calculation of SAE 1050 and SAE 1065 steel under random loading, International Journal of Fatigue 29 (2007), No. 9-11, pp. 1885-1892, DOI: 10.1016/j.ijfatigue.2007.01.005

13 P. Starke, F. Walther, D. Eifler: Fatigue assessment and fatigue life calculation of quenched and tempered SAE 4140 steel based on stress-strain hysteresis, temperature and electrical resistance measurements, Fatigue and Fracture of Engineering Materials & Structures 30 (2007), pp. 1044-1051, DOI: 10.1111/j.1460-2695. 2007.01174.x

14 G. Meneghetti: Analysis of the fatigue strength of a stainless steel based on the energy dissipation, International Journal of Fatigue 29 (2007), No.1, pp. 81-94, DOI: 10.1016/j.ijfatigue.2006.02.043

15 F. Walther, D. Eifler: Cyclic deformation behavior of steels and light-metal alloys,Materials Science and Engineering A 468–470 (2007), pp. 259-266, DOI: 10.1016/j.msea.2006.06.146

16 F. Walther, D. Eifler, U. Mosler, U. Martin: Deformation behaviour and microscopic investigations of cyclically loaded railway wheels and tires, International Journal of Materials Research 96 (2005), pp. 753-760, No. 7, DOI: 10.3139/146.101098

17 P. Starke, F. Walther, D. Eifler: "PHYBAL": a short-time procedure for a reliable fatigue-life calculation, Advanced Engineering Materials 12 (2010), No. 4, pp. 276-282, DOI: 10.1002/adem.200900344

18 J. D. Morrow: Cyclic plastic strain energy and fatigue of metals, ASTM-Internal Friction,

Abstract

Modellbasierte Korrelation zwischen elektrischer Widerstands- und Versetzungsdichteänderung von ermüdeten ICE R7 Radstahlproben. Die gewichtsoptimierte Bauteilauslegung sowie die zuverlässige Lebensdauerschätzung metallischer Werkstoffe und Bauteile erfordern ein umfassendes Verständnis der Ermüdungsprozesse und eine systematische Untersuchung des zugrundeliegenden Ermüdungsverhaltens. Dies wird umso wichtiger, wenn es sich um hochbeanspruchte Bauteile wie bspw. Räder des Hochgeschwindigkeitspersonenverkehrs handelt. Typischerweise werden mechanische Spannung-Dehnung-Hysteresis-Messungen und zunehmend unterschiedliche Arten der Temperatur- und elektrischen Widerstandsmessung eingesetzt, um das Ermüdungsverhalten zu charakterisieren. Insbesondere liefern hierbei elektrische Widerstandsmessungen einen deutlichen Mehrwert an Informationen, da sie bereits erste mikrostrukturelle Veränderungen detektieren können, die auf Versetzungsreaktionen zurückzuführen sind. Zusätzlich können elektrische Widerstandsmessungen bei Laststeigerungs- und Einstufenversuchen mit eingeschobenen lastfreien Haltezeiten sowie in Betriebslastversuchen zur Charakterisierung des Schädigungsfortschritts eingesetzt werden. Im Rahmen dieses Artikels wurden für den ICE-Vollradstahl R7 Kennwerte der elektrischen Widerstandsänderung ermittelt und beanspruchungs- bzw. lastspielzahlabhängig mit der Veränderung der röntgenografisch ermittelten Versetzungsdichte korreliert.

Damping and Cyclic Plasticity STP 378 (1964), pp. 45-87, DOI: 10.1520/STP43764S

Bibliography

DOI 10.3139/120.111202
Materials Testing
60 (2018) 7-8, pages 669-677

ISSN 0025-5300

The authors of this contribution

Dr.-Ing. Peter Starke, born in 1977, studied Mechanical Engineering at TU Kaiserslautern, Germany. Since 2002, he has been a research assistant at the Institute of Materials Science and Engineering (WKK) at TU Kaiserslautern, Germany. He received his engineering doctoral degree in 2007, working on "The fatigue life calculation of metallic materials under constant amplitude loading and service loading". From 2007 to 2012, he headed the research group "Fatigue life calculation" at WKK. Afterwards, he changed to the Fraunhofer IZFP in Saarbrücken, Germany. Since 2013 he is in the position of a senior research associate at the Chair of Non-Destructive Testing and Quality Assurance at Saarland University in Saarbrücken, Germany. His research is mainly focused on the use of non-destructive measurement techniques for the characterization of the fatigue behavior and the fatigue life calculation of metallic and non-metallic materials in the LCF-, HCF- and VHCF-regime as well as for the evaluation of defects and inhomogeneities in the materials microstructure.

Prof. Dr.-Ing. habil. Frank Walther, born in 1970, studied Mechanical Engineering majoring in Materials Science and Engineering at TU Kaiserslautern University, Germany. There he finished his PhD on the fatigue assessment of railway wheel steel in 2002 and his habilitation on physical measurement techniques for microstructural-based fatigue assessment and lifetime calculation of metals in 2007. At Schaeffler AG in Herzogenaurach, Germany, he was responsible for Public Private Partnership within Corporate Development from 2008 to 2010. Since 2010, he has been Professor for Materials Test Engineering (WPT) at TU Dortmund University, Germany. His research portfolio includes the determination of structure-property relationships in metal- and polymer-based materials and components under fatigue loading from the LCF to VHCF range, taking the influence of manufacturing and joining processes as well as service loading and corrosion deterioration into account.

Prof. Dr.-Ing. habil. Dietmar Eifler, born in 1949, got his PhD from the University of Karlsruhe, Germany. From 1991 to 1994, he was Professor at the University of Essen, Germany. From 1994 until 2015, he was Professor and from 2015 to 2017 Senior Research Professor at the Institute of Materials Science and Engineering at TU Kaiserslautern. His research activities are focused on the characterization of the fatigue behavior of metallic materials using mechanical, electrical, magnetic and acoustic as well as thermal measuring techniques in the LCF-, HCF- and VHCF regime.